Simulation Modelling Practice and Theory 126 (2023) 102774

Contents lists available at ScienceDirect

Simulation Modelling Practice and Theory

journal homepage: www.elsevier.com/locate/simpat

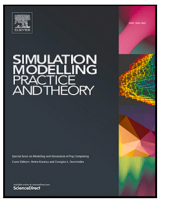

Robust optimization for functional multiresponse in 3D printing process

Zebiao Feng [a], Jianjun Wang [b,*], Xiaojian Zhou [a], Cuihong Zhai [b], Yizhong Ma [b]

[a] School of Management, Nanjing University of Posts and Telecommunications, Nanjing 210003, People's Republic of China
[b] Department of Management Science and Engineering, Nanjing University of Science and Technology, Nanjing 210094, People's Republic of China

ARTICLE INFO

Keywords:
3D printing
Functional multiresponse
Additive Gaussian process model
Robust optimization
Quality loss

ABSTRACT

Computer models are commonly used to simulate the functional relationships between inputs and outputs for quality design in 3D printing. However, the high-dimensional outputs of functional multiresponse make it challenging to develop the simulation model and perform robust optimization. This paper proposes a novel optimization method with an additive multiresponse Gaussian process model for dealing with functional multiresponse optimization problems. First, an additive covariance function is constructed to capture the correlation of the temporal inputs. Second, the Markov Chain Monte Carlo sampling technique is adopted to determine the simulation model and quantify the uncertainty. Finally, the optimization model is constructed by integrating the quality loss function and interval analysis method, and the Bayesian optimization algorithm is used to obtain the optimal solution. A numerical simulation example and a 3D printing case study are used to illustrate the effectiveness of the proposed method. The comparison results show that the responses of the proposed method are closer to the targets than the current ones, and all fall within the specified interval.

1. Introduction

Recently, additive manufacturing or 3D printing techniques have been increasingly used in industrial production for complex products or processes [1]. The additive manufacturing process obtains products by the layer fusion process with the 3D computer-aided simulation models. It can reduce the waste of material of the traditional manufacturing technique [2]. Meanwhile, 3D printing is easy to operate, low cost, and not limited by time and space of production, which has become a new alternative to traditional manufacturing processes [3]. While improving the quality of 3D printing products by robust optimization techniques is a challenging issue, specifically for the functional multiresponse, because of the high-dimensional outputs of simulation models. Therefore, it is meaningful to develop robust optimization techniques for functional multiresponse in 3D printing products.

The quality characteristics of 3D printing products include physical properties (e.g., tensile strength, heat resistance, and strain) and geometric properties (e.g., surface roughness and precision). Meanwhile, these quality characteristics are usually determined by process parameters (input parameter settings), such as laser power, scanning speed, layer height, and nozzle temperature. Therefore, research studies on a detailed microscopic level have focused on identifying appropriate process parameters and their settings to address the quality characteristics in 3D printing processes [4,5]. Robust parameter design is one of the most common quality improvement methods, mainly by selecting the input parameter settings to improve product quality [6,7]. Yadroitsev et al. [8] pointed out the parameter that most affected the stainless steel grade 904L powders was laser kilometer, followed by

* Corresponding author.
E-mail address: jjwang@njust.edu.cn (J. Wang).

https://doi.org/10.1016/j.simpat.2023.102774
Received 1 January 2023; Received in revised form 25 February 2023; Accepted 28 April 2023
Available online 4 May 2023
1569-190X/

powder layer thickness, scan speed, and particle size. Rayegani and Onwubolu [9] used the group method for data modeling and simulation for prediction purposes. Subsequently, Mohamed et al. [10] pointed out that determining the optimal process parameters is crucial to the mechanical properties of 3D products. They proposed a robust optimization method to select appropriate process parameters to improve mechanical properties for 3D printing products. Popescu et al. [11] found that different settings of process parameters impact the mechanical behavior of the products. Furthermore, Hashemi Sanatgar et al. [12] stated that the different combinations of process parameters (e.g., platform temperature, extruder temperature, and printing speed) can significantly affect the characterization of polymers to fabrics. Yadav et al. [13] investigated the influence of material density, infill density, and extrusion temperature on the mechanical properties of 3D printing products. Kamaal et al. [14] found that tensile property was significantly influenced by the infill percentage, building direction, and layer height of the fused deposition modeling. Lokesh et al. [15] studied the effect of 3D printing parameters (build orientation, Layer thickness, and raster angle) on the mechanical properties through the design of experiment by using the Taguchi approach. Afterward, ten Bhömer et al. [16] found that the air intake volume and the printing speed can affect the adhesion strength of 3D printed material on the fabric. With the complexity of product structure and appearance, robust optimization methods based on nonparametric simulation models are used to solve the quality improvement problems of 3D printing. McConaha and Anand [17] used the neural network model to develop the robust optimization method, compensating for the error deviation in the 3D printing process and improving the product quality. Most of the above studies with the traditional simulation models cannot effectively deal with the robust optimization problems in 3D printing because of the complex, nonlinear, or even functional responses.

Due to the time-consuming nature of the simulations, Gaussian process (GP) models are often used as response surfaces to estimate the relationship between input variables and outputs. The response surface based on the GP model has the advantages of high prediction accuracy and time-saving, which provides great convenience for realizing robust parameter design [18–20]. Tan and Wu [21] proposed a quadratic expected quality loss function based on the GP model and adopted the posterior probability analysis method to perform robust optimization. Subsequently, Costa and Lourenço [22] constructed the optimization model with the outputs of the GP model to evaluate the robustness of the optimal solution. Wang, Yuan, and Ng [23] considered the influence of input noise on the optimal results and used the stochastic simulation method to improve the robustness of the optimal solution. Then, Ouyang et al. [24] used the Monte Carlo simulation technique to obtain the optimal robust solution under data pollution. For high-dimensional response optimization problems, Zhang et al. [25] constructed the GP model with mixed input variables, which improves the prediction accuracy of simulation models. Kleijnen and Mehdad [26] pointed out that the variance estimator significantly underestimates the true variance, which may affect the performance of GP models. Feng et al. [27] further improved the prediction accuracy by calibrating the variance with the conditional simulation method. While most existing robust optimization methods with GP models cannot effectively deal with the optimization problems for the functional response.

Recently, it has received extensive attention from researchers on simulation modeling and robust optimization for functional response [28,29]. Conti and O'Hagan [30] developed the GP model using the separable covariance structure. They fixed some elements in the covariance matrix, significantly saving computational costs. Subsequently, Chen and Müller [31] proposed an additive model based on GP regression to make the mean function have the additive property. While their method can only be used for single-response regression prediction. Hung, Joseph, and Melkote [32] pointed out that fitting a functional response with a GP model is extremely challenging due to the computational cost of high-dimensional outputs. They developed a functional GP model by the Kronecker product to simplify the model structure. Jiang, Tan, and Tsui [33] proposed a separable GP modeling method based on the Cartesian product covariance structure to save the computational cost further. In addition, some researchers have tried using the GP model to deal with robust optimization problems in the 3D printing process. Cheng, Wang, and Tsung [34] proposed a bias compensation method based on the GP model to improve the shape fidelity of the 3D printing process. Khatri et al. [35] verified that the relationship between printing parameters and tensile strength is functional by using simulation analysis. While, most of the above studies cannot deal with the robust optimization with the functional multiresponse in 3D printing. Therefore, it is meaningful to develop the robust optimization method of functional multiresponse in 3D printing process.

In order to solve the robust optimization problems of functional multiresponse to improve the product quality in 3D printing process, a novel robust optimization model is proposed by integrating the Markov Chain Monte Carlo method and the additive GP modeling technique. The proposed additive GP covariance function makes the temporal input t as the additive form, which has the advantages of a more flexible model structure to simulate the functional multiresponse. In addition, interval analysis of functional multiresponse is adopted to qualify the model uncertainty, which improves the robustness and reliability of the optimal solution.

The remainder of the article is organized as follows. Section 2 provides the additive multiresponse GP modeling process and parameter estimation process. The proposed robust optimization method is given in Section 3. Section 4 illustrates the advantages of the proposed method through numerical simulation examples and the 3D printing case study. The work finishes with a discussion in Section 5 that provides further context for the results.

2. Modeling process

2.1. Functional multiresponse GP

Consider the multivariate GP model with m input variables are $\mathbf{x} = [x_1, \ldots, x_m]^{\mathrm{T}}, x_p = [a_p, t], a_p = [a_{p,1}, \ldots, a_{p,d}], p = 1, \ldots, m.$ $t = t_1, \ldots, t_f$ is a time factor that makes the output response functional. The n-dimension output response vector is $\mathbf{y} = [\mathbf{y}_1, \ldots, \mathbf{y}_n]^T$,

$\mathbf{y}_i = [\mathbf{y}_{i,1}, \ldots, \mathbf{y}_{i,m}], i = 1, \ldots, n$, $\mathbf{y}_{i,m} = [y_{i,m}^{t_1}, \ldots, y_{i,m}^{t_f}]$. The output of the input x_0 can be given by [33]

$$\begin{aligned} &\begin{bmatrix} \mathbf{y}_1(x_0) \\ \vdots \\ \mathbf{y}_n(x_0) \end{bmatrix} \sim \mathrm{N}\left(\begin{pmatrix} \mathbf{u}_1(x_0)|\mathbf{f}_1(x_0) \\ \vdots \\ \mathbf{u}_n(x_0)|\mathbf{f}_n(x_0) \end{pmatrix}, \begin{pmatrix} \xi_1 \\ \vdots \\ \xi_n \end{pmatrix} \right) \\ &\mathbf{y}_i(a_0) = \begin{bmatrix} y_{i,1}^{t_1}(a_0) & \cdots & y_{i,1}^{t_f}(a_0) \\ \vdots & \ddots & \vdots \\ y_{i,m}^{t_1}(a_0) & \cdots & y_{i,m}^{t_f}(a_0) \end{bmatrix}, i = 1, \ldots, n. \end{aligned}, \tag{1}$$

where $\mathbf{u}_i(x_0)$ represents the ith predicted response mean, $\mathbf{u}_i(x_0) = [\mathbf{u}_{i,1}(x_0), \ldots, \mathbf{u}_{i,m}(x_0)]$, $\mathbf{u}_{i,p}(a_0) = [\mathbf{u}_{i,p}^{t_1}(a_0), \ldots, \mathbf{u}_{i,p}^{t_f}(a_0)], p = 1, \ldots, m$. $\mathbf{F} = [\mathbf{f}_1, \ldots, \mathbf{f}_n]^{\mathrm{T}}$ is the prediction function, $\mathbf{f}_i = [f_{i1}, \ldots, f_{im}]$, $f_{ip} = [f_{ip}^{t_1}, \ldots, f_{ip}^{t_f}]$. $\xi_i = [\xi_i^{t_1}, \ldots, \xi_i^{t_f}]$ is the noise of the ith response. Consider a Gaussian prior for $\mathbf{f}_i$:

$$\mathbf{f}_i(x_0) \sim \mathrm{N}\left(\mathbf{m}_i(x_0), \mathbf{K}_i(x_0, \mathbf{x})\right), \tag{2}$$

where $\mathbf{m}_i(x_0)$ is the mean function or latent variable function, and it is always set as 0 . $\mathbf{K}_i(x_0, \mathbf{x})$ represents the covariance relationship between the input x_0 of the ith response and the observation $\mathbf{x}$.

2.2. Additive modeling

If there is no time factor x_t in the input variables, the modeling process can be as follows. The covariance relationship between x_0 and x_1 can be represented by the square exponential kernel function [36]:

$$k(x_0, x_1) = {\sigma_i}^2 \exp\left(-\sum_{k=1}^{d} (x_{0,k} - x_{1,k})^2 l_k^{-2}/2\right), \tag{3}$$

where ${\sigma_i}^2$ is the parameter to control the curve smoothness of ith response. l_k^{-2} is the parameter to determine the correlation of the kth input factor. The hyperparameters of the model are $\boldsymbol{\theta} = \{\boldsymbol{\sigma}, \boldsymbol{\xi}, \boldsymbol{l}\}$, $\boldsymbol{\sigma} = [\sigma_1, \ldots, \sigma_n]$, $\boldsymbol{\xi} = [\xi_1, \ldots, \xi_n]$, $\boldsymbol{l} = \{l_1, \ldots, l_d\}$.

The correlation between the x_0 of ith response and the x_1 of the jth response can be represented by

$$K(\mathbf{x}_0^i, \mathbf{x}_1^j) = \tau_{i,j}\sigma_i\sigma_j \exp\left(-\sum_{k=1}^{d} (x_{0,k} - x_{1,k})^2 l_k^{-2}/2\right), \tag{4}$$

where $\tau_{i,j} = \tau_{i,j}, i, j = 1, \ldots, n$ represent the correlation of responses i and j. To ensure the validity of the covariance matrix $[\mathbf{K}]_{i0,j1} = K(\mathbf{x}_0^i, \mathbf{x}_1^j)$ constructed by Eqs. (3) and (4), the $n \times n$ matrix $[\mathbf{T}]_{ij} = \tau_{i,j}$ must be the positive definite matrix with unit diagonal elements (PDUDE). The hypersphere decomposition method is used to construct the covariance matrix with the additional parameters $\boldsymbol{\omega}$, see Appendix A for details.

It should be noted that the above covariance matrices are mainly developed for continuous input factors, which cannot effectively deal with the case of the functional response with discontinuous factors. Meanwhile, as shown in Eq. (4), $\tau_{i,j}$ has been used to capture the correlation of different responses. If another parameter is adopted to capture the correlation of time factors, the covariance structure will be very complicated, and it will be very difficult to ensure the PDUDE of the covariance matrix. To this end, additive modeling methods are adopted to construct the covariance matrix with the time factors. First, the covariance matrices are constructed for different input factors (continuous input and time factor). And then, the covariance matrices are added together to form a new covariance matrix, which can capture the correlation of different inputs and outputs. The detailed additive process is described as follows.

The additive latent variable function of input $x_0 = [x_{0,1}, \ldots, x_{0,d}]$ can be given by

$$\mathbf{F}(x_0) = \mathbf{f}(a_0) + f(t) = f_1 + \cdots + f_d + f_t, \tag{5}$$

then, f_k $(k = 1, \ldots, d.)$ can be represented by

$$f_k \sim N(0, \mathbf{K}^k), \tag{6}$$

where $\mathbf{K}^k$ is given by

$$\mathbf{K}^k(x_{0,k}^i, x_{1,k}^j) = \tau_{i,j}\sigma_i\sigma_j \exp(-(x_{0,k} - x_{1,k})^2 l_k^{-2}/2), \tag{7}$$

where $x_{0,k}^i$ represents the kth factor of x_0 in the ith response. $x_{1,k}^j$ represents the kth factor of x_1 in the jth response. The additive covariance function can be represented as

$$\begin{aligned} \boldsymbol{\Psi} &= \mathbf{K}^1 + \cdots + \mathbf{K}^d + \mathbf{K}^t \\ &= \sum_{k=1}^{d} \mathbf{K}^k(x_{0,k}, \mathbf{x}_k) + \sum_{g=1}^{t_f} \mathbf{K}^t(t_g, \mathbf{t}) \\ &= \tau_{i,j}\sigma_i\sigma_j[\sum_{k=1}^{d} \exp(-(x_{0,k} - \mathbf{x}_k)^2 l_k^{-2}/2) + \sum_{g=1}^{t_f} \exp(-(t_g - \mathbf{t})^2 l_k^{-2}/2)] \end{aligned}. \tag{8}$$

Then, the conjugate prior at the input x_0 can be expressed as

$$\begin{bmatrix} f_1 \\ \vdots \\ f_t \\ \mathbf{F} \\ \mathbf{y} \end{bmatrix} \sim N\left(\begin{bmatrix} 0 \\ \vdots \\ \vdots \\ 0 \\ 0 \end{bmatrix}, \begin{bmatrix} \mathbf{K}^1 & & & \mathbf{K}^1 & \mathbf{K}^1 \\ & \ddots & & \vdots & \vdots \\ & & \mathbf{K}^t & \mathbf{K}^t & \mathbf{K}^t \\ \mathbf{K}^1 & \cdots & \mathbf{K}^t & \boldsymbol{\Psi} & \boldsymbol{\Psi} \\ \mathbf{K}^1 & \cdots & \mathbf{K}^t & \boldsymbol{\Psi} & \boldsymbol{\Psi}_y \end{bmatrix}\right), \tag{9}$$

where $\mathbf{F} \sim N(0, \boldsymbol{\Psi})$. $\boldsymbol{\Psi}_y = (\boldsymbol{\Psi}(x_0, x_0)|\theta + \xi^2\mathbf{I})$. For the model parameters $\theta = \{\sigma, \xi, l, \omega\}, \sigma = [\sigma_1, \ldots, \sigma_n]$, $\xi = [\xi_1, \ldots, \xi_n]$, $l = \{l_1, \ldots, l_d, l_{t_1}, \ldots, l_{t_f}\}$, the conditional distribution of $\mathbf{f}(x_0)$ can be expressed as

$$\mathbf{f}(x_0)|\mathbf{F}, \mathbf{x}, \mathbf{y}, \theta \sim \mathrm{N}(\boldsymbol{\Psi}_{\mathbf{x},x_0}\boldsymbol{\Psi}_{\mathbf{x},\mathbf{x}}^{-1}\mathbf{F}, \boldsymbol{\Psi}_{x_0,x_0} - \boldsymbol{\Psi}_{x_0,\mathbf{x}}\boldsymbol{\Psi}_{\mathbf{x},\mathbf{x}}^{-1}\boldsymbol{\Psi}_{\mathbf{x},x_0}). \tag{10}$$

Then, the output of the additive Gaussian process model is given by

$$\begin{aligned} \mathbf{u}(x_0) &= \boldsymbol{\Psi}(x_0, \mathbf{x}|\theta)(\boldsymbol{\Psi}^{-1}(\mathbf{x}, \mathbf{x}|\theta) + \xi^2\mathbf{I})^{-1}\mathbf{y} \\ \mathbf{s}(x_0) &= \boldsymbol{\Psi}(x_0, x_0|\theta) - \boldsymbol{\Psi}(x_0, \mathbf{x}|\theta)(\boldsymbol{\Psi}^{-1}(\mathbf{x}, \mathbf{x}|\theta) + \xi^2\mathbf{I})^{-1}\boldsymbol{\Psi}(\mathbf{x}, x_0|\theta) \end{aligned}, \tag{11}$$

where $\boldsymbol{\Psi}(x_0, \mathbf{x}|\theta) = K(x_0, \mathbf{x}^1|\theta), \ldots, K(x_0, \mathbf{x}^n|\theta)$, $\mathbf{x}^n$ is the observation vector of the nth response.

2.3. Parameter estimation

After determining the model structure mentioned in Section 2.2, the hyperparameters need to be estimated to obtain the model output. The marginal likelihood function is $p(\mathbf{y}|\mathbf{x}, \theta)$, and the hyperparameters are $\theta = \{\sigma, \xi, l, \omega\}$. The Markov Chain Monte Carlo sampling method introduced by Gelman et al. [37] is adopted to estimate the hyperparameters. The samples are obtained by $p(\theta|\mathbf{x}, \mathbf{y})$, and the joint posterior distribution of the model hyperparameters is given by

$$\begin{aligned} &\pi(\sigma, \xi, l, \omega|\mathbf{x}, \mathbf{y}) \propto \\ &\pi(\sigma)\pi(\omega)\pi(\xi)\pi(l)\left|\boldsymbol{\Psi}_{\mathbf{x},\mathbf{x}} + \xi^2\mathbf{I}\right|^{-\frac{1}{2}} \exp\left\{-\tfrac{1}{2}(\mathbf{y} - \mathbf{f}(\mathbf{x}))'(\boldsymbol{\Psi}_{\mathbf{x},\mathbf{x}} + \xi^2\mathbf{I})^{-1}(\mathbf{y} - \mathbf{f}(\mathbf{x}))\right\}. \end{aligned} \tag{12}$$

The priors of the hyperparameters are as follows [37]:

$$\pi(\log(\sigma_k^2)) \propto 1, k = 1, \ldots, m. \tag{13}$$

$$\pi(l_h) \propto \frac{\Gamma((\nu_t+1)/2)}{\Gamma(\nu_t/2)\sqrt{\nu_t\pi\sigma_t^2}}\left(1 + \frac{(l_h-\mu_t)^2}{\nu_t\sigma_t^2}\right)^{-(\nu_t+1)/2}, \mu_t = 0, \nu_t = 4, \sigma_t^2 = 1, h = 1, \ldots, d, t_1, \ldots, t_f. \tag{14}$$

$$\pi(\log(\xi_k^2)) \propto 1, k = 1, \ldots, m. \tag{15}$$

$$\pi(\log(\omega_e)) \propto 1, e = 1, \ldots, m(m-1)/2. \tag{16}$$

The sampling process of parameter estimation can be seen in Appendix B for details. By repeating a large number of the sampling process, the means of unknown parameters can be used to determine the additive multiresponse GP model. Then, the prediction mean and variance in Eq. (11) can be obtained. Then, the predicted output can be used to construct the robust optimization model for the functional response.

3. Robust optimization model

3.1. Quality loss

Taguchi defined quality loss as "The deviation between the quality characteristics and the specified target will lead to quality loss. the greater the deviation value, the greater the loss". He proposed the expected quality loss function to measure product quality further. To deal with the multiresponse robust optimization problems, Ko, Kim, and Jun [38] proposed the multivariate quality loss function:

$$QL(\mathbf{x}_0) = (\mathbf{u}(\mathbf{x}_0) - \mathbf{T})^{\mathrm{T}}\mathbf{C}(\mathbf{u}(\mathbf{x}_0) - \mathbf{T}) + trace[\mathbf{C}\Sigma_{\mathbf{u}(\mathbf{x}_0)}], \tag{17}$$

where $\mathbf{u}(\mathbf{x}_0)$ is the predicted response mean vector. $\mathbf{T}$ is the target of the output response. $\Sigma_{\mathbf{u}(\mathbf{x}_0)}$ is the variance–covariance matrix at input $\mathbf{x}_0$. $\mathbf{C}$ is the cost matrix. There are some useful methods to obtain the cost matrix $\mathbf{C}$, such as the methods introduced by Pignatiello [39]. Calculating the elements in the cost matrix is not the main work here. Then, without loss of generality, the cost matrix is given by

$$\mathbf{C} = \begin{bmatrix} 0.5 & 0.05 & \cdots & 0.05 \\ 0.05 & \ddots & \ddots & \vdots \\ \vdots & \ddots & \ddots & 0.05 \\ 0.05 & \cdots & 0.05 & 0.5 \end{bmatrix}_{n\times n}, \tag{18}$$

where n is the number of the output responses.

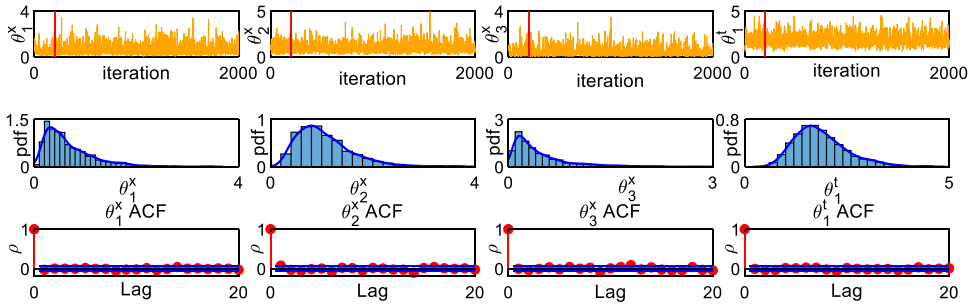

Fig. 1. The sampling results of the model parameter θ. θ_i^x and θ_i^t represent the parameter of the ith response.

3.2. Robust optimization

As mentioned in Section 3.1, the commonly used quality loss (QL) functions are mainly proposed for single-response or multiresponse optimization problems. While, there is no way to deal directly with the robust parameter design for functional responses. The quality characteristic requirement of the functional response is usually a functional boundary. For example, the stress of the 3D printing product is a functional curve with the printing speed, corresponding to the target of the stress is also a functional curve. To this end, this paper proposes an optimization model by integrating the quality loss function and the nonlinear constraint to perform the robust optimization of functional responses:

$$\begin{aligned} QL(\mathbf{x}_0) &= \sum_{k=1}^{n} [(\mathbf{u}_k(\mathbf{x}_0) - \mathbf{T}_k)^{\mathrm{T}} \mathbf{C}_k (\mathbf{u}_k(\mathbf{x}_0) - \mathbf{T}_k) + trace(\mathbf{C}_k \Sigma^k_{\mathbf{u}_k(\mathbf{x}_0)})], \\ s.t. \quad & CI_k(\mathbf{x}_0) \in S_k, \end{aligned} \tag{19}$$

where $\mathbf{u}_k(\mathbf{x}_0)$ is the predicted response of the kth response at input $\mathbf{x}_0$. $\mathbf{T}_k$ is the kth target of the response. S_k is the specified target interval of the kth response. CI_k is the confidence interval of the kth response, and can be obtained by the interval analysis technique, see Appendix C for details. Cost matrix $\mathbf{C}_k$ is set as same as in Section 3.1. The Bayesian optimization technique introduced by Martinez-Cantin [40] has the advantage of sequential optimization, which is more accurate for GP models. Therefore, the Bayesian optimization algorithm in Matlab is adopted to minimize Eq. (19) to obtain the optimal solution. Besides, the optimization model with the confidence interval can effectively quantify the response uncertainty and improve the robustness and reliability of the optimal solution.

3.3. Steps of the modeling process

The modeling process of the proposed robust optimization model based on the additive MGP model can be summarized as follows.

Step 1 Determine the experiment and collect the data.

Step 2 Construct the additive covariance matrix to capture the correlation of input variables.

Step 3 Use the hypersphere decomposition method to capture the correlation between functional multiresponse.

Step 4 Adopt the Markov Chain Monte Carlo sampling technique to estimate the model parameters and determine the model structure.

Step 5 Construct the optimization model by integrating the quality loss function and nonlinear interval constraint.

Step 6 Minimize the objective function Eq. (19) by using the Bayesian optimization algorithm to obtain the optimal solution.

4. Case study

In this section, a numerical simulation example is used to illustrate the effectiveness of the proposed method. Then, the proposed method is applied to the 3D printing process to improve the robustness and reliability of the product.

4.1. Numerical simulation example

In this example, the Bohachevsky function is adopted to illustrate the capability of the proposed method for $3d$ input. There are three input variables x_1, x_2, and x_3. There is also an input t to make the responses functional. The responses are y_1, y_2, and y_3. The test function is given by [41]

$$\begin{cases} y_1 = t(x_1^2 + 2x_2^2 - 0.3\cos(\pi/2 + \pi x_1/3) - 0.4\cos(\pi/2 + \pi x_2/4) + 0.7x_3) + t^2 \\ y_2 = t(x_1^2 + 2x_2^2 - 0.3\sin(\pi x_1/3)\sin(\pi x_2/4) + 0.3x_3) + t^2 \\ y_3 = t(x_1^2 + 2x_2^2 - 0.3\cos(\pi/2 + \pi x_1/3 + \pi x_2/4) + 0.5x_3) + t^2 \end{cases} \tag{20}$$

where $x_i \in [-1, 1], i = 1, \ldots, 3$. $t = 1, 2, 3, 4, 5$. The 30 training points are obtained by the Latin square design, which is commonly used in computer experiment and machine learning. The experiment data can be seen in Appendix D. After that, the additive multiresponse

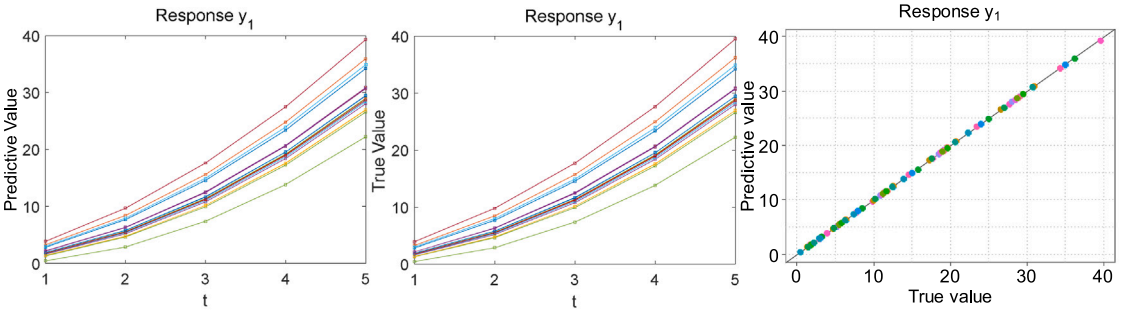

(a) The predicted and true values of y_1.

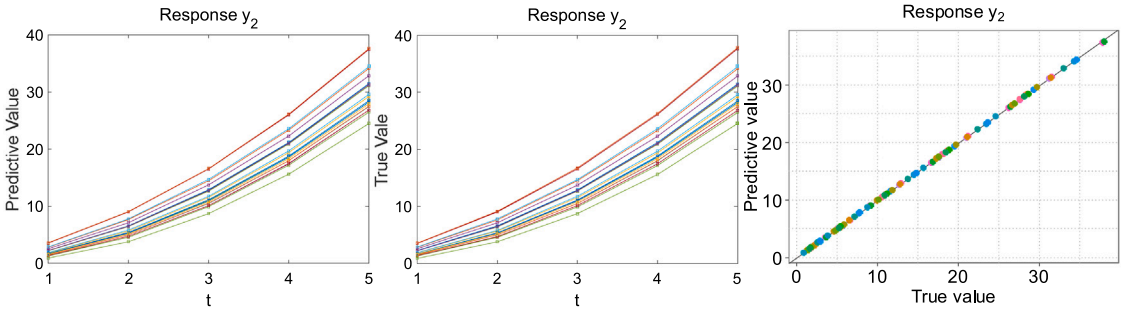

(b) The predicted and true values of y_2.

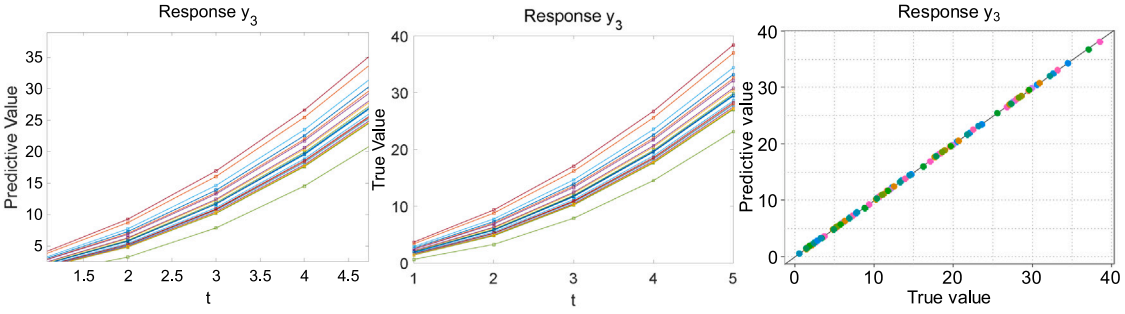

(c) The predicted and true values of y_3.

Fig. 2. The predicted and true values of the three responses.

GP model introduced in Section 2 is used to fit the functional response surface with the experiment data. The Markov Chain Monte Carlo sampling technique is used to estimate the hyperparameters. The number of iterations for estimating the unknown parameter is 2000, the first 200 of which are taken as burn-in. The traceplot, probability density, and autocorrelation for convergence diagnosis of model parameters (e.g., θ) are given in Fig. 1. It can be seen in Fig. 1 that the Markov Chain Monte Carlo algorithm of the proposed optimization process is convergence. Besides, the 20 test points are used to verify the model prediction accuracy, and the predicted and true values of the test points are given in Fig. 2 to illustrate the prediction accuracy of the proposed model. It should be pointed out that the time variable t is taken as the x-axis, and each curve in Fig. 2 corresponds to the response of a test point x. Besides, It can be seen from Fig. 2 that the response curves are functional with time t, and the proposed method obtains the predicted responses with high accuracy.

To further illustrate the advantages of the proposed method, the predicted results of the other three methods are given for comparison. They are the GP model only has one response (OGP) [42], the multi-task GP model (MTGP) with sparse technique [43], and the multiresponse GP (MRGP) model with dynamic hierarchical technique [44]. Meanwhile, the RMSE (Root Mean Square Errors) and MAE (Mean Absolute Errors) are used to evaluate the prediction accuracy of different methods. RMSE and MAE can be

Table 1
Comparison results of MAE and RMSE for different methods.

Method	MAE			RMSE		
	y_1	y_2	y_3	y_1	y_2	y_3
OGP	0.0773	0.0621	0.0670	0.1308	0.1020	0.1130
MTGP	0.0416	0.0402	0.0425	0.0866	0.0838	0.0893
MRGP	0.1044	0.1040	0.1040	0.1710	0.1711	0.1707
PM	0.0148	0.0109	0.0132	0.0304	0.0271	0.0286

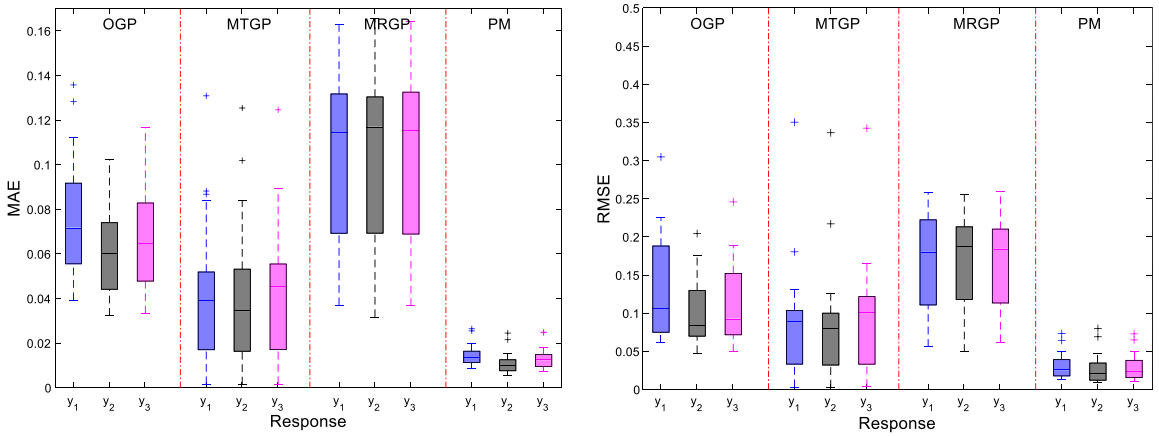

(a) MAE. (b) RMSE.

Fig. 3. MAE and RMSE of different methods.

obtained by

$$\mathrm{RMSE} = \frac{1}{\mathrm{RN}} \sqrt{\frac{1}{m} \sum_{i=1}^{m} \left(\bar{y}\left(x_i\right) - y\left(x_i\right)\right)^2}. \tag{21}$$

$$\mathrm{MAE} = \frac{1}{\mathrm{RN} \times \mathrm{m}} \sum_{i=1}^{m} \left|\bar{y}\left(x_i\right) - y\left(x_i\right)\right|. \tag{22}$$

where m is the number of the test points, $m = 20$. RN is the number of the calculation process, RN = 20. $\bar{y}$ is the predicted response. y is the true response.

The MAEs and RMSEs of different methods are given in Table 1 and Fig. 3. The MRGP method fixes some parameters in the covariance function before parameter estimation to save computing costs. Hence the prediction accuracy of MRGP is relatively poor, and it obtains the worst predicted results with the largest RMSEs and MAEs for the responses. Moreover, because the correlation between different output responses is not considered when constructing the covariance matrix, the prediction accuracy of OGP and MTGP is also worse. Hence MAEs and RMSEs of the above method are larger than the proposed one. It can be seen in Fig. 3 that the minimum of MAEs and RMSEs of MTGP are smaller than that of PM, but its mean values are greater than the PM, which means the MTGP is not robust compared with the PM. Besides, OGP needs to construct 15 models to predict the three responses at 5 locations ($t = 1, \ldots, 5$), which greatly increases the difficulty and cost of the modeling process. The proposed method (PM) obtains a relatively high prediction accuracy, and the MAEs of responses are 0.0157, 0.0119, and 0.0143; the RMSEs are 0.0595, 0.0558, and 0.0573. Based on the above analysis, the proposed method has the highest prediction accuracy in this example, followed by the MTGP, OGP, and MRGP methods. In particular, the proposed method not only accurately obtains the prediction results, but also provides a more direct way to construct the response surface for the functional multiresponse. Furthermore, the Matérn kernel is also a flexible and popular kernel function for building GP models. The comparison results of the Matérn kernel and square exponential kernel are detailed in Appendix E.

4.2. 3D printing process

A real case study of the 3D printing process introduced by Waseem et al. [45] is used to illustrate the proposed method. There are three input variables: Layer height x_1 (mm), Infill x_2 (%), and Patterns t, where $t = 1, 2, 3$ represent the linear pattern, hexagonal pattern, and diamond pattern, respectively. The code levels of input variables are given in Table 2. The responses of the printing process are creep rate y_1 (l/s) and the rupture time y_2 (h). y_1 is the smaller-the-better type characteristic, and y_2 is the

Table 2
Code levels of input variables.

Input parameter	Symbols	True value(Code level)		
Layer Height	x_1	0.1(−1)	0.2(0)	0.3(1)
Infill	x_2	10(−1)	55(0)	100(1)
Patterns	t	Linear(1)	Hexagonal(2)	Diamond(3)

Table 3
The experimental design and results.

No.	Input		y_1			y_2		
	x_1	x_2	t_1	t_2	t_3	t_1	t_2	t_3
1	0.5994	−0.1294	0.1090	0.1005	0.1075	1.3137	2.1186	1.3068
2	−0.6399	−0.7824	0.1084	0.0844	0.1100	1.2845	2.0660	1.2968
3	0.9373	−0.4233	0.1083	0.1045	0.1065	1.3351	2.1026	1.3309
4	−0.1787	0.4271	0.1077	0.0886	0.1072	1.2874	2.1675	1.2775
5	0.2548	0.1229	0.1090	0.0958	0.1079	1.2991	2.1379	1.2906
6	−0.5483	0.7364	0.1053	0.0810	0.1053	1.2803	2.2002	1.2689
7	0.0245	−0.1040	0.1097	0.0937	0.1094	1.3088	2.1334	1.3052
8	−0.9297	−0.6545	0.1059	0.0781	0.1081	1.2737	2.0757	1.2863
9	0.4860	0.9143	0.1049	0.0939	0.1026	1.2260	2.1314	1.2049

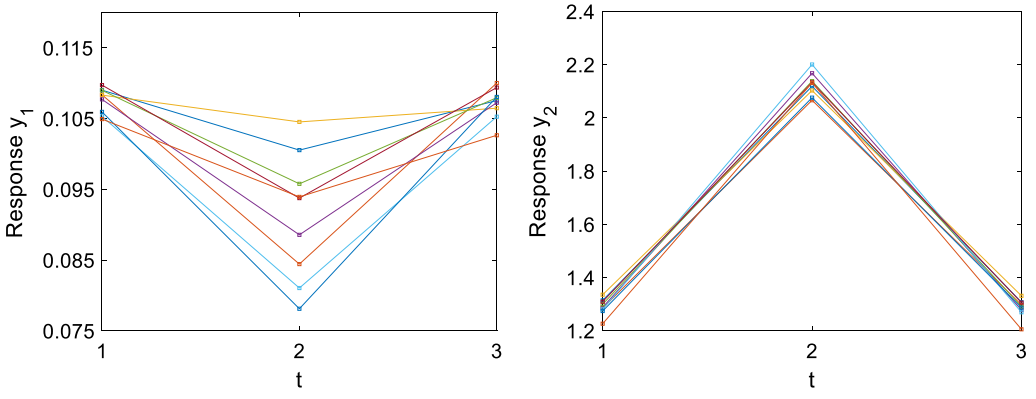

(a) y_1. (b) y_2.

Fig. 4. The true curves of the 9 training points.

larger-the-better type characteristic. The targets of y_1 and y_2 are $T_1 = [0, 0, 0]$ and $T_2 = [3, 3, 3]$, respectively. The upper of y_1 is $U = [0.1055, 0.0950, 0.1075]$, and the lower of y_2 is $L = [1.28, 2.13, 1.26]$. The relationship between the inputs and outputs is given by

$$y_1 = \begin{cases} 0.1094 + 0.001x_1 - 0.003x_2 - 0.004x_1^2 - 0.001x_2^2 - 0.001x_1x_2, \mathrm{t} = 1. \\ 0.093 + 0.014x_1 - 0.004x_2 - 0.004x_1^2 - 0.001x_2^2 - 0.001x_1x_2, \mathrm{t} = 2. \\ 0.109 - 0.001x_1 - 0.004x_2 - 0.004x_1^2 - 0.001x_2^2 - 0.001x_1x_2, \mathrm{t} = 3. \end{cases} \tag{23}$$

$$y_2 = \begin{cases} 1.305 + 0.005x_1 - 0.037x_2 - 0.008x_1^2 - 0.026x_2^2 - 0.054x_1x_2, \mathrm{t} = 1. \\ 2.14 - 0.025x_1 + 0.056x_2 - 0.008x_1^2 - 0.026x_2^2 - 0.054x_1x_2, \mathrm{t} = 2. \\ 1.30 - 0.002x_1 - 0.052x_2 - 0.007x_1^2 - 0.025x_2^2 - 0.054x_1x_2, \mathrm{t} = 3. \end{cases} \tag{24}$$

where $x_i \in [-1, 1], i = 1, 2$. $t = 1, 2, 3$. The Latin square design technique can obtain more information with fewer repetitions, and it is used to generate 9 training points. The experimental design and results are shown in Table 3 and Fig. 4.

The purpose of robust parameter design in this case study is to find the optimal parameter settings in the feasible region to make y_1 as small as possible and y_2 as large as possible. The response surface model is constructed with the experimental data in Table 3 using the process described in Section 2. Then, the robust optimization model can be given by

$$\begin{aligned} \mathrm{QL}(x) &= \sum_{i=1}^{2} k_i \left[(y_i - T_i)' C (y_i - T_i) + trace(C_i V_i) \right] \\ s.t. \quad & \mathrm{CI}(y_1) \le \mathrm{U}, \quad \mathrm{CI}(y_2) \ge \mathrm{L}, \end{aligned} \tag{25}$$

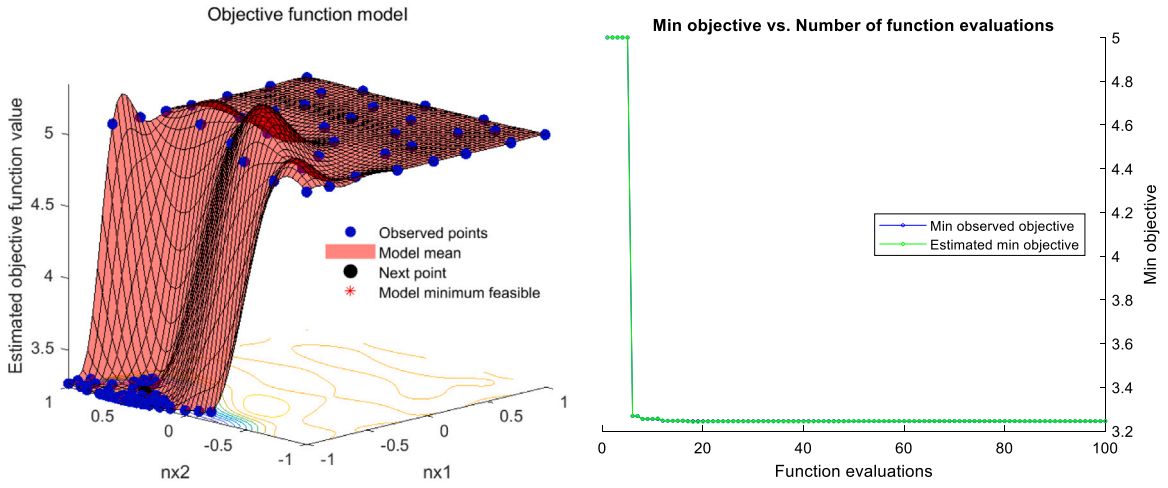

(a) Objective function model. (b) Evaluations.

Fig. 5. Iteration of the Bayesian optimization procedure.

Table 4
Optimization results of different methods.

Method	Input		y_1			y_2			QL	CD
	x_1	x_2	t_1	t_2	t_3	t_1	t_2	t_3		
OGP	1	−0.5440	*0.1083*	*0.1054*	0.1064	1.3438	*2.0982*	1.3413	3.1720	4.5368
MTGP	−1	0.5004	0.1031	0.0732	0.1042	1.2940	2.2055	1.2897	3.2452	4.4914
MRGP	−0.6127	0.2111	*0.1067*	0.0822	0.1074	1.2969	2.1700	1.2935	3.2648	4.5359
OQL	1	−0.9999	*0.1094*	*0.1070*	*0.1080*	1.3670	*2.0790*	1.3720	**3.1105**	4.5064
PM	−0.9995	0.5467	0.1030	0.0731	0.1041	1.2935	2.2093	1.2886	3.2449	**4.4887**
Limitation	–	–	0.1055	0.0950	0.1075	1.28	2.13	1.26	–	–

where k_i is the coefficient of the cost for ith response, without loss of generality, let $k_1 = k_2 = 0.5$ here. y_i represents the prediction of the ith response. T_i represents the target of the ith response. V_i is the variance–covariance matrix of the ith response. $CI(y_i)$ is the confidence interval of the ith response. The Bayesian optimization algorithm in Matlab is used to minimize Eq. (25), the number of the max objective evaluations is set as 100, and other tuning parameters remain the default. The optimization iterative process is shown in Fig. 5. The results of OGP, MTGP, MRGP, and OQL methods are also given for comparison in Table 4.

Table 4 gives the optimal inputs, true responses, quality loss (QL), and the cumulative deviation (CD) between the true responses and targets. The OQL method does not use interval analysis to consider the output response uncertainty. Hence the responses y_1 and y_2 of OQL ($y_1 = [0.1094, 0.1070, 0.1080]$) cannot meet the specific constraint ($U = [0.1055, 0.0950, 0.1075]$). Meanwhile, it can be seen in Table 4 that responses of y_1 at t_1 and t_2 ($y_1 = [0.1083, 0.1054, 0.1064]$) of OGP also cannot meet the specific constraint because of its poor prediction performance. Similarly, due to the poor accuracy the response y_1 of MRGP at t_1 in Table 4 is also larger than the specific constraint U. Therefore, although the same optimization method is used, the above methods cannot obtain the optimal result within the specified interval due to the insufficient prediction accuracy of the regression model. Correspondingly, the proposed method and MTGP method can obtain the optimal solution with the response within the specified (i.e., L and U) constraints due to their high prediction accuracy for functional multiresponse.

On the other hand, compared with the OQL method, the PM obtains a larger quality loss (QL = 3.2449), while the CD (CD = 4.4887) of PM is smaller, which means PM obtains the optimal solution closest to the targets. Besides, due to poor prediction accuracy, the responses of OQL cannot meet the requirement of the specific constraint. Besides, compared with the MRGP method, the PM obtains the more robust optimal solution with the smaller QL and CD. Moreover, The CD of OGP performs worst, which means it obtains the optimal solution with the responses furthest from the targets. Therefore, due to the poor prediction accuracy, the optimal solutions of other methods perform worse than the proposed one. Therefore the proposed method obtains a more robust optimal solution than other ones.

The proposed method provides a new way to deal with the robust optimization and quality improvement of functional responses in the 3D printing process. In fact, the proposed method with the additive covariance structure can accurately capture the correlation between input variables and the correlation between functional multiresponse. In addition, the proposed method can effectively deal with the robust optimization problems for the functional response, which is not directly for the commonly used GP models. The proposed robust optimization model with interval analysis obtains the optimal solution that considers the requirements of the specific constraint and improves the robustness of the optimization results.

5. Conclusions

Most current simulation models and robust optimization methods cannot effectively deal with the functional multiresponse optimization problems in the 3D printing process. In this paper, a novel additive GP model is developed to perform the regression prediction for functional multiresponse and robust optimization in the 3D printing process, which is the main contribution of this paper. Besides, the modeling framework of combining the additive structure and the Markov Chain Monte Carlo technique provides a new way to simulate functional multiresponse relationships. In addition, the interval analysis technique of functional multiresponse significantly improves the robustness and reliability of the optimization results.

The comparison results of the numerical example show that the proposed method can obtain the functional multiresponse surface model with smaller MAE and RMSE than others. Besides, it can be seen from the case study that the proposed method can effectively reduce quality loss and better meet the requirements of the specific target limits. Therefore, the proposed method can help practitioners solve quality improvement problems with functional responses in 3D printing.

This paper develops an additive GP model to effectively deal with regression prediction and robust optimization for functional responses. The proposed method provides a more flexible and effective way to deal with robust optimization for functional multiresponse, which can be used to improve product quality in 3D printing. The proposed method ignores the effect of second-order and interaction terms in robust optimization. However, the second-order and interaction terms may also affect product quality in 3D printing. Therefore, developing the variable selection method for the proposed additive GP model to identify important factors can further improve prediction accuracy and save computing costs. Besides, this paper only considers two responses (creep rate and rupture time) to verify the effectiveness of the proposed simulation and robust optimization method. It is necessary to consider the relationship between stress–strain in the quality design of the 3D printing process, which will be the focus of our future research.

Declaration of competing interest

The authors declare that they have no known competing financial interests or personal relationships that could have appeared to influence the work reported in this paper.

Data availability

Data will be made available on request.

Acknowledgments

This work was supported by the National Natural Science Foundation of China [grant numbers 72171118, 71771121, 71931006, 71872088].

Appendix A. Hypersphere decomposition

The covariance matrix of the GP model must meet the PDUDE requirements. First, the matrix $\mathbf{T}$ must be performed the Cholesky decomposition:

$$\mathbf{T} = \mathbf{L}\mathbf{L}^{\mathrm{T}}, \tag{A.1}$$

where $\mathbf{L} = \{l_{r,s}\}, 1 \le s < r \le n$ is a $n \times n$ lower triangular matrix. Then, each row vector $(l_{r,1}, \dots, l_{r,s})$ in $\mathbf{L}$ can be represents as the point coordinate on the unit sphere:

$$l_{r,s} = \begin{cases} 1, r = s = 1 \\ \cos\omega_{r,s}, s = 1 \\ \cos\omega_{r,s} \Pi_{t=1}^{s-1} \sin\omega_{r,t}, s = 2, \dots, r-1 \\ \Pi_{t=1}^{r-1} \sin\omega_{r,t}, 1 < r = s \le n \end{cases}, \tag{A.2}$$

where $\omega_{r,s} \in (0, \pi)$. Let $\boldsymbol{\omega} = \{\omega_{r,s}\}_{r>s}$ is a $m \times m$ lower triangular matrix, and only specify the elements except for the diagonal in the lower triangular matrix $\mathbf{L}$. The feasible range of $\boldsymbol{\omega}$ is $(0, \pi)^{m(m-1)}/2$. By Eqs. (A.2)–(A.1), the matrix $\mathbf{T}$ can be given by

$$\mathbf{T} = \mathbf{L}\mathbf{L}^{\mathrm{T}} = \begin{bmatrix} 1 & l_{1,2} & \cdots & l_{1,m} \\ l_{2,1} & l_{2,1}^2 + l_{2,2}^2 & \cdots & l_{2,m} \\ \vdots & \vdots & \ddots & \vdots \\ l_{m,1} & l_{m,2} & \cdots & l_{m,1}^2 + \cdots + l_{m,m}^2 \end{bmatrix}. \tag{A.3}$$

Then, the correlation between the output responses p and q can be obtained by $\tau_{p,q} = [\mathbf{T}]_{pq}, p, q = [1, \dots, n]$. Meanwhile, it can be seen from Eq. (A.3) $\mathbf{T}$ is a $m \times m$ PDUDE matrix. It should be pointed out that constructing the covariance matrix by the hypersphere decomposition method needs the addition hyperparameters $\boldsymbol{\omega} = [\omega_1, \dots, \omega_{m(m-1)}/2]$.

Appendix B. Parameter estimation

The steps of the parameter estimation process for the proposed additive GP model can be summarized as follows. The joint posterior distribution for the parameters is

$$\begin{aligned}&\pi(\boldsymbol{\sigma},\boldsymbol{\xi},\boldsymbol{l},\boldsymbol{\omega}|\mathbf{x},\mathbf{y})\propto\\&\pi(\boldsymbol{\sigma})\pi(\boldsymbol{\omega})\pi(\boldsymbol{\xi})\pi(\boldsymbol{l})\left|\boldsymbol{\Psi}_{\mathbf{x},\mathbf{x}}+\xi^2\mathbf{I}\right|^{-\frac{1}{2}}\exp\left\{-\tfrac{1}{2}(\mathbf{y}-\mathbf{f}(\mathbf{x}))'(\boldsymbol{\Psi}_{\mathbf{x},\mathbf{x}}+\xi^2\mathbf{I})^{-1}(\mathbf{y}-\mathbf{f}(\mathbf{x}))\right\}.\end{aligned}\tag{B.1}$$

where the noninformative priors for model parameters can be seen in Section 2.3.

Let $\{\sigma_k^j, l_h^j, \xi_k^j, \omega_e^j\}$ be the jth sample from the posterior distribution. To obtain the $j+1$ sample, we follow the following steps:

Steps 1: Update the parameter $\boldsymbol{\sigma}$ by drawing a new value form its conditional distribution: $p(\sigma_k|\mathbf{f},\boldsymbol{\xi},\boldsymbol{l},\boldsymbol{\omega},\mathbf{x},\mathbf{y})\propto U(0,+\infty)$.

Steps 2: Update the parameter $\boldsymbol{l}$ by drawing a new value form its conditional distribution: $p(l_h|\mathbf{f},\boldsymbol{\sigma},\boldsymbol{\xi},\boldsymbol{\omega},\mathbf{x},\mathbf{y})\propto t_4(0,1)$.

Steps 3: Update the parameter $\boldsymbol{\xi}$ by drawing a new value form its conditional distribution: $p(\xi_k|\mathbf{f},\boldsymbol{\sigma},\boldsymbol{l},\boldsymbol{\omega},\mathbf{x},\mathbf{y})\propto U(0,+\infty)$.

Steps 4: Update the parameter $\boldsymbol{\omega}$ by drawing a new value form its conditional distribution: $p(\omega_k|\mathbf{f},\boldsymbol{\sigma},\boldsymbol{l},\boldsymbol{\xi},\mathbf{x},\mathbf{y})\propto U(0,+\infty)$.

Steps 5: Update the parameter $\mathbf{f}$ by drawing a new value form its conditional distribution: $p(\mathbf{f}|\boldsymbol{\sigma},\boldsymbol{l},\boldsymbol{\xi},\boldsymbol{\omega},\mathbf{x},\mathbf{y})\propto N\left(\frac{\sum_{i=1}^m \frac{\mathbf{y}(\mathbf{x}^i)}{\xi_i^2}}{\sum_{i=1}^m \frac{1}{\xi_i^2}},\frac{1}{\sum_{i=1}^m \frac{1}{\xi_i^2}}\right)$.

The model hyperparameters are obtained by repeating Steps (1–5) for a large number of iterations.

Appendix C. Interval analysis

In engineering practice, the output response is usually limited to a specified interval to meet the quality characteristics. Meanwhile, the interval analysis technique effectively limits the output response to a specified interval for multiresponse optimization problems. When the confidence level (CL) of the confidence region is at least $(1-\alpha)\times 100\%$, the confidence region can be given by Bonferroni's inequality:

$$\begin{aligned}&Pr\{(y_1,y_2,\ldots,y_d)\in CR\}\\&=Pr\{y_1\in CI_1,y_2\in CI_2,\ldots,y_d\in CI_d\}\\&\geq 1-[\Pr\{y_1\in CI_1\}+\Pr\{y_2\in CI_2\}+\cdots+\Pr\{y_d\in CI_d\}]\\&=1-\alpha/d\times d\end{aligned}\tag{C.1}$$

where y is the predicted response. d is the number of responses. CI_i is the confidence interval of the ith response.

The posterior distribution of the ith output response for GP model can be given by

$$y_i(\mathbf{x}_0)\sim N(u_i(\mathbf{x}_0),v_i(\mathbf{x}_0)),\tag{C.2}$$

where $u_i(\mathbf{x}_0)$ is the ith predicted response. v_i is the ith predicted variance. The confidence interval of the ith response can be given by

$$\Pr\{y_i(\mathbf{x}_0)\in CI_i\}=\Pr\{y_i\in(y_{iL},y_{iU})\}=1-\alpha.\tag{C.3}$$

By Eq. (C.2), the confidence interval of response y_i is given by

$$\Pr\{y_i\in u_i(\mathbf{x}_0)\pm z_{\alpha/2}\sqrt{v_i(\mathbf{x}_0)}\}=1-\alpha.\tag{C.4}$$

For the d output responses, the CL of each response must be as least $(1-\alpha/d)\times 100\%$ to make the CL of the confidence region is $(1-\alpha)\times 100\%$. The confidence interval of the response y_i is given by

$$CI_{y_i}=[u_i(\mathbf{x}_0)-z_{\alpha/2d}\sqrt{v_i(\mathbf{x}_0)},u_i(\mathbf{x}_0)+z_{\alpha/2d}\sqrt{v_i(\mathbf{x}_0)}],\tag{C.5}$$

where $z_{\alpha/2d}$ is the $\alpha/2d$ quantile of the standard normal distribution. Then, Eq. (C.5) can be used to constrain the bounds of the functional response, which will further improve the robustness and reliability of the optimal solution.

Appendix D. Experimental data

See Table D.1.

Appendix E. Results for the Matérn kernel

The Matérn kernel is widely used to construct the GP model [36]. The covariance function with the Matérn kernel can be given by

$$k_v(x_i,x_j)=\sigma^2\frac{2^{1-v}}{\Gamma(v)}\left(\sqrt{2v}r\right)^v K_v\left(\sqrt{2v}r\right),\tag{E.1}$$

Table D.1
Experimental design and data.

No.	Input			y_1					y_2					y_3				
	x_1	x_2	x_3	x_3^1	x_3^2	x_3^3	x_3^4	x_3^5	x_3^1	x_3^2	x_3^3	x_3^4	x_3^5	x_3^1	x_3^2	x_3^3	x_3^4	x_3^5
1	0.80	0.83	−0.68	3.01	8.02	15.03	24.03	35.04	2.68	7.36	14.04	22.73	33.41	2.98	7.96	14.94	23.92	34.89
2	0.10	−0.78	−0.97	1.35	4.69	10.04	17.38	26.73	1.95	5.90	11.84	19.79	29.74	1.59	5.18	10.77	18.37	27.96
3	0.88	0.59	0.71	3.38	8.77	16.15	25.53	36.91	2.58	7.15	13.73	22.30	32.88	3.12	8.24	15.36	24.47	35.59
4	0.94	0.09	0.88	2.80	7.61	14.41	23.21	34.02	2.15	6.31	12.46	20.61	30.77	2.61	7.22	13.83	22.44	33.05
5	−0.98	0.67	0.76	3.35	8.71	16.06	25.42	36.77	3.23	8.47	15.70	24.93	36.17	3.11	8.23	15.34	24.45	35.56
6	−0.28	−0.95	−0.27	2.33	6.66	12.99	21.32	31.64	2.74	7.47	14.21	22.94	33.68	2.48	6.96	13.45	21.93	32.41
7	−0.65	0.29	0.30	1.71	5.42	11.12	18.83	28.54	1.73	5.45	11.18	18.91	28.64	1.61	5.23	10.84	18.46	28.07
8	0.65	−0.65	−0.90	1.64	5.28	10.92	18.56	28.20	2.10	6.20	12.29	20.39	30.49	1.88	5.75	11.63	19.51	29.39
9	0.82	−0.37	0.08	2.11	6.23	12.34	20.45	30.56	2.03	6.07	12.10	20.14	30.17	2.15	6.29	12.44	20.58	30.73
10	−0.87	0.14	−0.43	1.30	4.60	9.90	17.20	26.51	1.69	5.39	11.08	18.78	28.47	1.37	4.73	10.10	17.46	26.83
11	0.49	−0.26	−0.36	1.19	4.38	9.57	16.76	25.95	1.30	4.59	9.89	17.18	26.48	1.29	4.57	9.86	17.14	26.43
12	−0.25	−0.47	0.85	1.88	5.75	11.63	19.50	29.38	1.73	5.46	11.20	18.93	28.66	1.75	5.50	11.26	19.01	28.76
13	−0.45	−0.67	−0.51	1.41	4.81	10.22	17.63	27.04	1.88	5.76	11.64	19.51	29.39	1.59	5.19	10.78	18.37	27.97
14	−0.83	0.64	−0.24	2.29	6.58	12.87	21.16	31.46	2.53	7.07	13.60	22.13	32.67	2.27	6.54	12.81	21.08	31.34
15	0.56	0.00	−0.13	1.39	4.79	10.18	17.58	26.97	1.28	4.56	9.84	17.11	26.39	1.42	4.84	10.26	17.68	27.10
16	0.02	−0.85	0.20	2.35	6.70	13.05	21.40	31.75	2.51	7.03	13.54	22.06	32.57	2.37	6.74	13.11	21.48	31.85
17	0.32	−0.44	0.53	1.83	5.65	11.48	19.31	29.14	1.69	5.38	11.06	18.75	28.44	1.76	5.51	11.27	19.02	28.78
18	0.71	0.45	0.66	2.72	7.43	14.15	22.86	33.58	2.04	6.08	12.12	20.16	30.20	2.51	7.02	13.53	22.04	32.54
19	0.44	−0.93	0.59	3.20	8.41	15.61	24.82	36.02	3.19	8.39	15.58	24.77	35.97	3.14	8.28	15.42	24.56	35.70
20	0.39	−0.33	−0.86	0.79	3.58	8.37	15.16	23.95	1.15	4.29	9.44	16.59	25.73	0.99	3.98	8.97	15.96	24.95
21	−0.11	−0.19	0.02	1.00	4.00	9.00	16.01	25.01	1.08	4.17	9.25	16.34	25.42	1.01	4.03	9.04	16.05	25.07
22	−0.35	−0.09	−0.58	0.60	3.20	7.80	14.39	22.99	0.96	3.92	8.87	15.83	24.79	0.72	3.45	8.17	14.89	23.61
23	0.18	−0.02	−0.75	0.56	3.12	7.67	14.23	22.79	0.81	3.62	8.43	15.23	24.04	0.71	3.42	8.13	14.84	23.55
24	−0.17	0.91	−0.06	2.85	7.71	14.56	23.41	34.27	2.70	7.41	14.11	22.82	33.52	2.81	7.62	14.43	23.24	34.05
25	0.24	−0.57	0.18	1.73	5.47	11.20	18.94	28.67	1.79	5.59	11.38	19.17	28.96	1.74	5.48	11.21	18.95	28.69
26	−0.53	0.97	−0.13	3.19	8.38	15.57	24.76	35.95	3.23	8.46	15.69	24.92	36.16	3.16	8.32	15.48	24.64	35.80
27	−0.80	0.35	0.98	2.45	6.91	13.36	21.82	32.27	2.24	6.48	12.71	20.95	31.19	2.21	6.43	12.64	20.85	31.07
28	−0.03	0.25	0.43	1.50	4.99	10.49	17.99	27.48	1.26	4.51	9.77	17.03	26.29	1.39	4.78	10.17	17.56	26.95
29	−0.68	0.75	−0.61	2.17	6.34	12.51	20.69	30.86	2.50	7.00	13.50	22.01	32.51	2.23	6.46	12.69	20.93	31.16
30	−0.54	0.51	0.38	2.08	6.16	12.23	20.31	30.39	1.99	5.98	11.97	19.97	29.96	1.96	5.91	11.87	19.83	29.78

Table E.1
Comparison results of the square exponential kernel and Matérn kernel.

Method	MAE			RMSE		
	y_1	y_2	y_3	y_1	y_2	y_3
SEK	0.0148	0.0109	0.0132	0.0304	0.0271	0.0286
MK	0.0125	0.0173	0.0324	0.0194	0.0249	0.0496

where $r = \left(\sum_{k=1}^{d} \frac{(x_{i,k}-x_{j,k})^2}{l_k^2}\right)^{1/2}$. The parameter υ governs the smoothness of the process, and K_ν is a modified Bessel function. The Matérn covariance functions can be represented more simpler when υ is a half-integer. The Matérn covariance functions with $\upsilon = 3/2$ and $\upsilon = 5/2$ are:

$$k_{\upsilon=3/2}(x_i, x_j) = \sigma^2\left(1+\sqrt{3}r\right)\exp\left(-\sqrt{3}r\right), \tag{E.2}$$

$$k_{\upsilon=5/2}(x_i, x_j) = \sigma^2\left(1+\sqrt{5}r+\frac{5r^2}{3}\right)\exp\left(-\sqrt{5}r\right). \tag{E.3}$$

To simplify, we give the results with $\upsilon = 3/2$ of example 1 in Section 4.1 to illustrate the effectiveness of the Matérn kernel. The results are given in Table E.1.

It can be seen in Table 1 that the Matérn kernel (MK) does not have obvious advantages over the square exponential kernel (SEK). From the perspective of MAE, y_1 of MK is smaller than that of SEK. y_2 and y_3 of MK are larger than SEK. From the perspective of RMSE, y_1 and y_2 of MK are smaller than that of SEK. y_3 of MK is larger than that of SEK. Therefore, the square exponential kernel is adopted to construct the GP model for robust parameter design in the paper.

References

[1] S. Ford, T. Minshall, Invited review article: Where and how 3D printing is used in teaching and education, Addit. Manuf. 25 (2019) 131–150.

[2] Q. Huang, J. Zhang, A. Sabbaghi, T. Dasgupta, Optimal offline compensation of shape shrinkage for three-dimensional printing processes, IIE Trans. 47 (5) (2014) 431–441.

[3] Y. Ling, J. Ni, J. Antonissen, H.B. Hamouda, J.V. Voorde, M.A. Wahab, Numerical prediction of microstructure and hardness for low carbon steel wire Arc additive manufacturing components, Simul. Model. Pract. Theory 122 (2023) 102664.

[4] K. Li, S. Yan, Y. Zhong, W. Pan, G. Zhao, Multi-objective optimization of the fiber-reinforced composite injection molding process using Taguchi method, RSM, and NSGA-II, Simul. Model. Pract. Theory 91 (2019) 69–82.
[5] J.D. Kechagias, A. Tsiolikas, M. Petousis, K. Ninikas, N. Vidakis, L. Tzounis, A robust methodology for optimizing the topology and the learning parameters of an ANN for accurate predictions of laser-cut edges surface roughness, Simul. Model. Pract. Theory 114 (2022) 102414.
[6] M. Azaouzi, N. Lebaal, G. Rauchs, S. Belouettar, Optimal design of multi-step stamping tools based on response surface method, Simul. Model. Pract. Theory 24 (2012) 1–14.
[7] E.J. Chen, M. Li, Design of experiments for interpolation-based metamodels, Simul. Model. Pract. Theory 44 (2014) 14–25.
[8] I. Yadroitsev, I. Yadroitsava, P. Bertrand, I. Smurov, Factor analysis of selective laser melting process parameters and geometrical characteristics of synthesized single tracks, Rapid Prototyp. J. 18 (3) (2012) 201–208.
[9] F. Rayegani, G.C. Onwubolu, Fused deposition modelling (FDM) process parameter prediction and optimization using group method for data handling (GMDH) and differential evolution (DE), Int. J. Adv. Manuf. Technol. 73 (1–4) (2014) 509–519.
[10] O.A. Mohamed, S.H. Masood, J.L. Bhowmik, Optimization of fused deposition modeling process parameters: a review of current research and future prospects, Adv. Manuf. 3 (1) (2015) 42–53.
[11] D. Popescu, A. Zapciu, C. Amza, F. Baciu, R. Marinescu, FDM process parameters influence over the mechanical properties of polymer specimens: A review, Polym. Test. 69 (2018) 157–166.
[12] R. Hashemi Sanatgar, C. Campagne, V. Nierstrasz, Investigation of the adhesion properties of direct 3D printing of polymers and nanocomposites on textiles: Effect of FDM printing process parameters, Appl. Surf. Sci. 403 (2017) 551–563.
[13] D. Yadav, D. Chhabra, R.K. Garg, A. Ahlawat, A. Phogat, Optimization of FDM 3D printing process parameters for multi-material using artificial neural network, Mater. Today: Proc. 21 (2020) 1583–1591.
[14] M. Kamaal, M. Anas, H. Rastogi, N. Bhardwaj, A. Rahaman, Effect of FDM process parameters on mechanical properties of 3D-printed carbon fibre–PLA composite, Progr. Addit. Manuf. 6 (2021) 63–69.
[15] N. Lokesh, B. Praveena, J.S. Reddy, V.K. Vasu, S. Vijaykumar, Evaluation on effect of printing process parameter through Taguchi approach on mechanical properties of 3D printed PLA specimens using FDM at constant printing temperature, Mater. Today: Proc. 52 (2022) 1288–1293.
[16] M. ten Bhömer, D. Tate, S. Wang, F. Campanile, Y. Chen, Application of robust design techniques for 3D printing on textiles, in: Proceedings of the AHFE 2019 International Conference on Additive Manufacturing, Modeling Systems and 3D Prototyping, Springer, 2020, pp. 153–165.
[17] M. McConaha, S. Anand, Additive manufacturing distortion compensation based on scan data of built geometry, J. Manuf. Sci. Eng. 142 (6) (2020) 061001.
[18] J.P. Kleijnen, Kriging metamodeling in simulation: A review, European J. Oper. Res. 192 (3) (2009) 707–716.
[19] Z. Feng, J. Wang, Y. Ma, Y. Tu, Robust parameter design based on Gaussian process with model uncertainty, Int. J. Prod. Res. 59 (9) (2021) 2772–2788.
[20] H.D. Karatza, Performance of gang scheduling strategies in a parallel system, Simul. Model. Pract. Theory 17 (2) (2009) 430–441.
[21] M.H.Y. Tan, C.F.J. Wu, Robust design optimization with quadratic loss derived from Gaussian process models, Technometrics 54 (1) (2012) 51–63.
[22] N.R. Costa, J. Lourenço, Gaussian process model - an exploratory study in the response surface methodology, Qual. Reliab. Eng. Int. 32 (7) (2016) 2367–2380.
[23] H. Wang, J. Yuan, S.H. Ng, Gaussian process based optimization algorithms with input uncertainty, IISE Trans. 52 (4) (2019) 377–393.
[24] L. Ouyang, M. Han, Y. Ma, M. Wang, C. Park, Simulation optimization using stochastic kriging with robust statistics, J. Oper. Res. Soc. (2022) http://dx.doi.org/10.1080/01605682.2022.2055498.
[25] Q. Zhang, P. Chien, Q. Liu, L. Xu, Y.L. Hong, Mixed-input Gaussian process emulators for computer experiments with a large number of categorical levels, J. Qual. Technol. 53 (4) (2021) 410–420.
[26] J.P.C. Kleijnen, E. Mehdad, Estimating the variance of the predictor in stochastic Kriging, Simul. Model. Pract. Theory 66 (2016) 166–173.
[27] Z. Feng, J. Wang, Y. Ma, X. Zhou, Multi-response robust optimization using GP model with variance calibration, Comput. Ind. Eng. 169 (2022) 108299.
[28] R. Al-Aomar, Incorporating robustness into Genetic Algorithm search of stochastic simulation outputs, Simul. Model. Pract. Theory 14 (3) (2006) 201–223.
[29] J.V.S. do Amaral, J.A.B. Montevechi, R.d.C. Miranda, W.T.d.S. Junior, Metamodel-based simulation optimization: A systematic literature review, Simul. Model. Pract. Theory 114 (2022) 102403.
[30] S. Conti, A. O'Hagan, Bayesian emulation of complex multi-output and dynamic computer models, J. Statist. Plann. Inference 140 (3) (2010) 640–651.
[31] K. Chen, H.-G. Müller, Modeling conditional distributions for functional responses, with application to traffic monitoring via gps-enabled mobile phones, Technometrics 56 (3) (2014) 347–358.
[32] Y. Hung, V.R. Joseph, S.N. Melkote, Analysis of computer experiments with functional response, Technometrics 57 (1) (2015) 35–44.
[33] F. Jiang, M.H.Y. Tan, K.-L. Tsui, Multiple-target robust design with multiple functional outputs, IISE Trans. 53 (9) (2020) 1052–1066.
[34] L.W. Cheng, A.D. Wang, F. Tsung, A prediction and compensation scheme for in-plane shape deviation of additive manufacturing with information on process parameters, IISE Trans. 50 (5) (2018) 394–406.
[35] B. Khatri, K. Lappe, D. Noetzel, K. Pursche, T. Hanemann, A 3D-printable polymer-metal soft-magnetic functional composite-development and characterization, Materials (Basel) 11 (2) (2018) 189.
[36] C.K.I. Williams, C.E. Rasmussen, Gaussian Processes for Machine Learning, MIT Press, Cambridge, 2006.
[37] A. Gelman, H.S. Stern, J.B. Carlin, D.B. Dunson, A. Vehtari, D.B. Rubin, Bayesian Data Analysis, Chapman and Hall/CRC, 2013.
[38] Y.H. Ko, K.J. Kim, C.H. Jun, A new loss function-based method for multiresponse optimization, J. Qual. Technol. 37 (1) (2005) 50–59.
[39] J.J. Pignatiello, Strategies for robust multiresponse quality engineering, IIE Trans. 25 (3) (1993) 5–15.
[40] R. Martinez-Cantin, Bayesopt: A Bayesian optimization library for nonlinear optimization, experimental design and bandits, J. Mach. Learn. Res. 15 (1) (2014) 3735–3739.
[41] J. Xing, Y. Luo, Z. Gao, A global optimization strategy based on the Kriging surrogate model and parallel computing, Struct. Multidiscip. Optim. 62 (1) (2020) 405–417.
[42] T. Zafar, Y. Zhang, Z. Wang, An efficient Kriging based method for time-dependent reliability based robust design optimization via evolutionary algorithm, Comput. Methods Appl. Mech. Engrg. 372 (113386) (2020) 1–24.
[43] R. Dürichen, T. Wissel, F. Ernst, M.A.F. Pimentel, D.A. Clifton, A. Schweikard, A unified approach for respiratory motion prediction and correlation with multi-task Gaussian Processes, in: IEEE International Workshop on Machine Learning for Signal Processing, 2014.
[44] Z. Chen, B. Wang, A.N. Gorban, Multivariate Gaussian and Student-t process regression for multi-output prediction, Neural Comput. Appl. 32 (8) (2019) 3005–3028.
[45] M. Waseem, B. Salah, T. Habib, W. Saleem, M. Abas, R. Khan, U. Ghani, M.U.R. Siddiqi, Multi-response optimization of tensile creep behavior of PLA 3D printed parts using categorical response surface methodology, Polymers (Basel) 12 (12) (2020) 2962.